COMPUTERS AND BIOMEDICAL RESEARCH **24,** 273–295 (1991)

Automated Detection of Breast Tumors Using the Asymmetry Approach

TIN-KIT LAU* AND WALTER F. BISCHOF†

**Department of Computing Science and †Department of Psychology, University of Alberta, Edmonton, Alberta, Canada T6G 2E9*

Received April 3, 1990

A method for automated detection of breast tumors in mammograms is presented. The method uses the asymmetry principle: Strong structural asymmetries between corresponding regions in the left and right breast are taken as evidence for the possible presence of a tumor in that region. Asymmetry detection is achieved in two steps. First, mammograms are aligned, compensating for possible differences in size and shape between the two breasts. Second, asymmetry between corresponding positions is determined using a combination of several asymmetry measures, each responding to different types of asymmetries. Results obtained with a set of mammograms indicate that this method can improve the sensitivity and reliability of systems for automated detection of breast tumors.

I. INTRODUCTION

Breast cancer is one of the leading cancers. About 10% of all women develop breast cancer and about 25% of all cancers diagnosed in women are breast cancers (*1*). Although effective prevention is not possible, early detection can at least reduce the chance of breast cancers from becoming incurable. Mammography has been shown to be the most effective and reliable method for early cancer detection (*2*).

Two different techniques are used in the interpretation of mammograms. The first technique consists of a systematic search of each mammogram for visual patterns symptomatic of tumors. For example, a bright, approximately circular blob with hazy boundary might indicate the presence of a circumscribed mass (*2, 3*). The second technique, the asymmetry approach, consists of a systematic comparison of corresponding regions in the left and right breast. Significant structural asymmetries between the two regions can indicate the possible presence of a tumor.

Mammogram interpretation is both time-consuming and difficult, requiring the expertise of trained radiologists. This stands at odds with the recommendation that mammography be performed at regular intervals to reduce the incidence of lethal breast cancers. However, with recent advances in medical image

0010-4809/91 $3.00

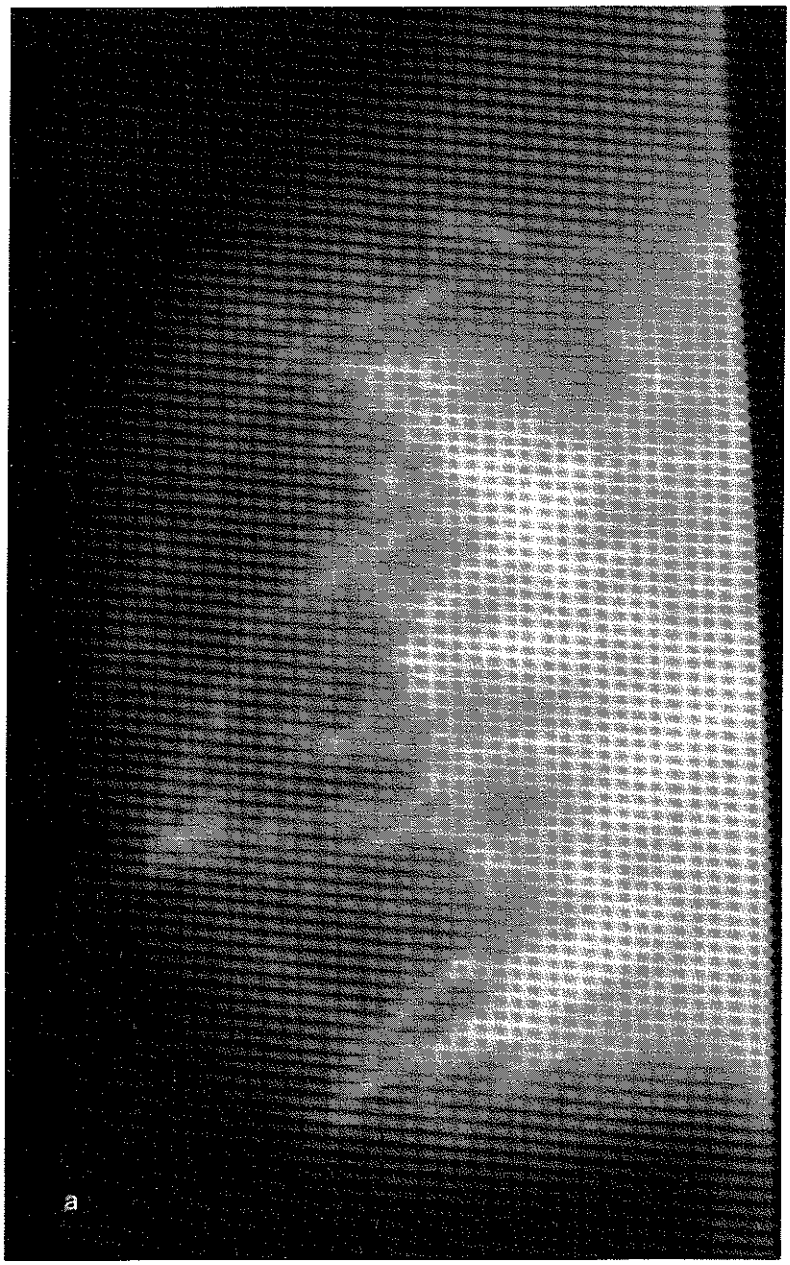

PLATE 1. Mammograms of the left (a) and right (b) breast. A tumor is present in the right breast at the position indicated by the two white lines. (The visible contours in (b) are an artifact of the printed reproduction and were not present in the original image.)

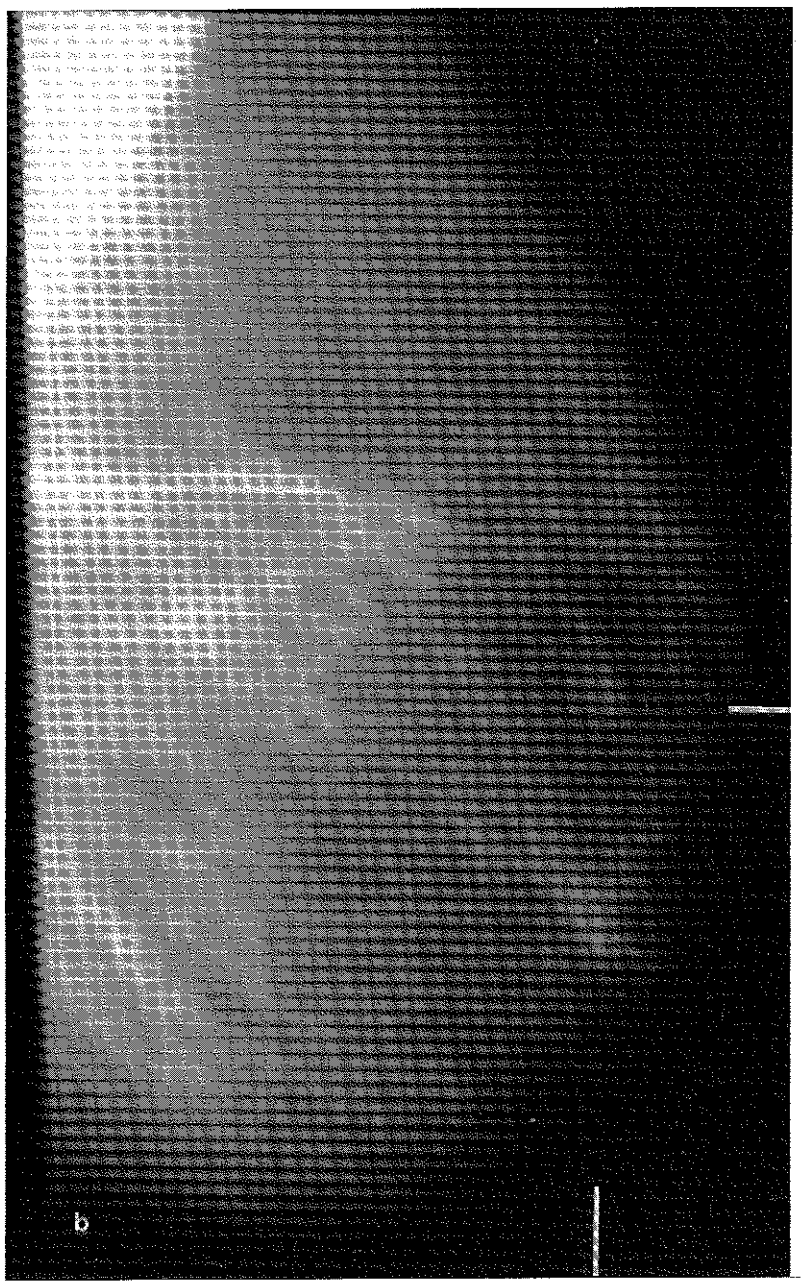
b

processing it has become feasible to design automated diagnosis systems, or, on a more modest level, to design systems that can aid radiologists in mammogram interpretation.

Several systems for automated mammogram interpretation have been proposed in the past. They differ both with respect to their goals and with respect to the techniques used to achieve these goals. Some systems (*4–6*) use texture measures to characterize the appearance of local regions within mammograms. Regions that have a markedly different appearance from the rest of the breast are considered possible tumor sites. In a similar way, Magnin *et al.* (*7*) use textural measures to characterize the general appearance of mammograms for assessing the risk of developing breast cancer. Other systems are designed to detect specific types of tumors, such as circumscribed masses (*3*), stellate tumors (*8*), or microcalcifications (*9*). Detection performance of these systems is generally better than the more general systems, since they can use tumor-specific characteristics both for the detection of tumors and for the elimination of non-tumors. Finally, some systems (*10,11*) are designed not to detect but to classify tumors at *known* positions. Diagnostic decisions of these systems are based upon sets of textural measures and their performance is usually excellent, approaching the performance of expert radiologists.

None of these systems is reliable enough to be used in clinical applications. However, all systems use methods that may be incorporated into a clinically useful system. The system described in the present article uses yet another method, the asymmetry approach, for detecting possible tumor locations in mammograms. The reason for considering this approach is not that we expect this method to be superior to other approaches. On the contrary, methods that attempt to detect specific tumors, are likely to give a better performance. The method presented here can, however, provide clues about the presence of tumors that are not available to other methods and thus it provides another building block for a clinically useful system. In fact, the system presented here is part of a project with the goal of developing a clinically useful system for mammographic tumor detection and classification (*3, 8*).

The strategy of the asymmetry detection system can be described as follows. Given a pair of identical-view mammograms of the left and right breast (see Plate 1), detect all structural asymmetries between corresponding positions in the left and right breast. Significant asymmetries are taken as evidence for the possible presence of a tumor.

A closer inspection of the mammograms shown in Plate 1 reveals several difficulties for the asymmetry approach. First, due to natural asymmetry, and due to the mammographic recording procedure, the shapes of the left and right breast do not match (apart from the mirror transformation). Defining corresponding positions in both breasts becomes therefore a nontrivial task. Second, the global appearance (brightness, contrast, etc.) of the two breasts may differ, usually due to variations in the recording procedure. Third,

asymmetries exist not only at the tumor position but also in the appearance of healthy breast tissue at corresponding locations in the two breasts. The asymmetry method thus has to discriminate tumor-related asymmetries from naturally occurring asymmetries. Finally, the tumor in the right breast of Plate 1 can be detected without using the asymmetry method, i.e., by analyzing the visual pattern in the right breast only. It is thus not clear what performance one can ideally expect of a system that uses *only* the asymmetry principle. The system described here should, at least partially, provide an answer to this question.

In the following we present a detailed account of the asymmetry method. We first present a method for mapping corresponding positions between the left and right breasts (Section II). Then we present and discuss several asymmetry measures (Section III). The results obtained with our method are illustrated using the mammograms in Plate 1. In the last section we present experimental results obtained with a set of mammograms, and we discuss the advantages and drawbacks of our approach (Section IV).

II. Mammogram Alignment

Before we can discuss methods for detecting asymmetries between corresponding regions in the left and right breasts, we must discuss methods for determining corresponding positions. There exist natural asymmetries, both in shape and in anatomic structure, between the two breasts. Further shape distortions are introduced through the mammographic recording procedure. For these reasons, it is impossible to define an exact correspondence between positions. However, a definition of exact correspondence is not a necessary requirement of this technique.

A simple method for aligning mammograms was proposed in (*10*), where mammograms are aligned using translations and rotations only, ignoring any differences in size and shape. A much more elaborate alignment method is the unwarping algorithm proposed in (*12*). This method requires the manual input of control-points distributed over the whole breast area. These points are then used to triangulate the breast area, with separate interpolation functions being applied in each region triangle. Although this method potentially allows a very precise mapping of positions, the time required for entering a large number of control-points manually precludes its use in a system intended for mass screening. It is also unclear to what extent reliable control-point extraction can be automated.

We have opted for a method midway between the two methods just presented. Its design was influenced by two considerations. First, we assume that the two breast areas to be aligned differ not only in global position and orientation, but also in shape and size. Second, we believe that no automatic alignment method works in all cases. In cases where automatic alignment fails, the alignment process should be controlled interactively, and user input in such cases should

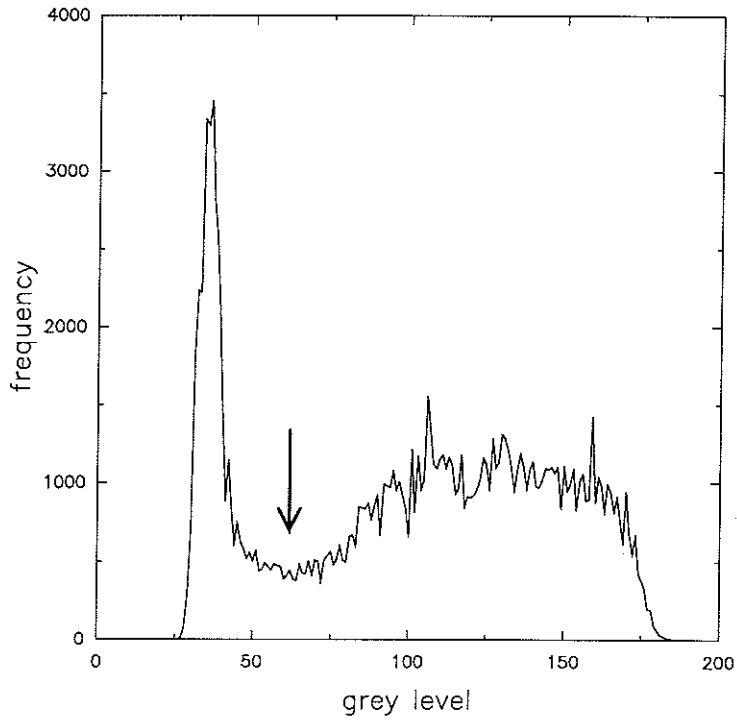

FIG. 1. Grey-level histogram of the mammogram in Plate 1a. The arrow indicates the position of the threshold for segmenting the breast area from the background.

be minimal. The proposed method aligns the breast areas using only three control-points on the boundary for guiding the alignment process. In the following we discuss all steps of this alignment process.

A. Digitization

Film mammograms were digitized with a camera at a resolution of 512 × 480 pixels and 256 grey levels. All mammograms were digitized at *approximately* the same orientation. Lettering, such as patient numbers or dates, were covered to make subsequent processing somewhat easier. No enhancement method was applied to the digitized mammograms, apart from simple grey-level stretching.

B. Breast Area Segmentation

First, the breast area must be segmented from the darker background. The grey-level histogram of the left mammogram in Plate 1 is shown in Fig. 1. It shows a clear bimodal distribution, indicating that the grey-level values of the breast area and of the background are distributed over different ranges. This allows simple thresholding to be used for segmenting the breast area from the

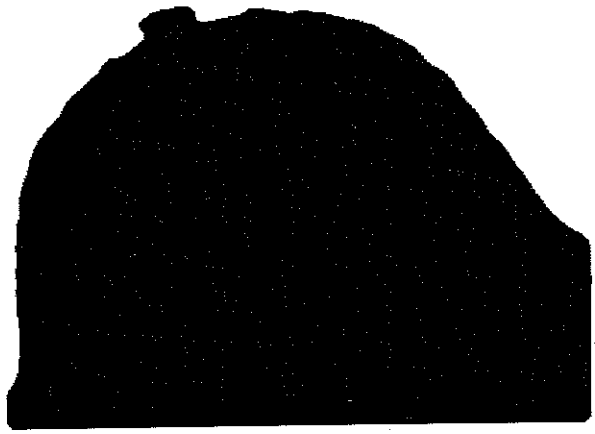

FIG. 2. Smoothed binary breast area map m_s of the mammogram in Plate 1a.

background, with the threshold T set to the grey level corresponding to the trough between the two peaks of the grey-level histogram.

The binary map $m(x,y)$ of the breast area can then be defined as

$$m(x,y) = \begin{cases} 1, & M(x,y) \geq T \\ 0, & M(x,y) < T, \end{cases} \quad [1]$$

where $M(x,y)$ denotes the digitized mammogram. Because simple thresholding produces a noisy boundary, an averaging filter is used to obtain a smooth binary map of the breast area. Let the averaging filter $a_2(x,y)$ be defined as

$$a_2(x,y) = \begin{cases} (2n+1)^{-2}, & |x| \leq n, |y| \leq n \\ 0, & \text{otherwise.} \end{cases} \quad [2]$$

Then the smoothed binary map $m_s(x,y)$ of the breast area is defined as

$$m_s(x,y) = \begin{cases} 1, & a_2(x,y) * m(x,y) \geq \frac{1}{2} \\ 0, & a_2(x,y) * m(x,y) < \frac{1}{2}, \end{cases} \quad [3]$$

where $a * b$ denotes the convolution of a and b. The smoothed binary map of the left mammogram in Plate 1, obtained using an averaging kernel with $n = 5$, is shown in Fig. 2. The binary breast area map m_s is used both for mammogram alignment and for defining the breast areas in the methods discussed in Section III.

C. Control-Point Extraction

The breast boundary curve can be easily extracted from the binary breast area map m_s. Let $b = \{(x_i,y_i), 0 \leq i < n_b\}$ be this (closed) boundary curve. On this curve three control-points are to be located, namely the nipple-point and

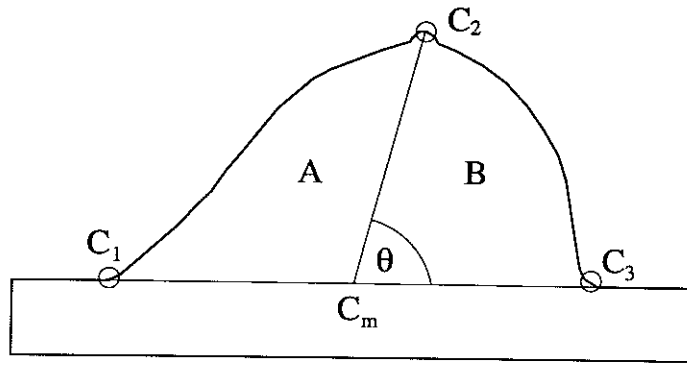

FIG. 3. Schematic outline of a breast area with three control-points, C_1, C_2, and C_3, used for alignment of mammograms. Also shown are the baseline $\overline{C_1C_3}$ and the centerline $\overline{C_mC_2}$ with an angle θ to the baseline. The two regions A and B are transformed independently.

the two corner-points between the breast boundary and the chest wall (Fig. 3). The control-points can be characterized as corners, i.e., as points of high curvature, on a smooth breast boundary curve. Inspection of the binary breast area map m_s (Fig. 2) shows that the boundary curve b is too noisy for obtaining these three control-points reliably. Therefore the curve b is further smoothed using a large one-dimensional averaging filter. Let

$$a_1(i) = \begin{cases} (2n + 1)^{-1}, & |i| \leq n \\ 0, & \text{otherwise} \end{cases} \qquad [4]$$

(in our implementation $n = 15$). Then the smooth boundary curve is defined as $b_s = \{(x_i^*, y_i^*), 0 \leq i < n_b\}$ with $x_i^* = a_1 * x$ and $y_i^* = a_1 * y$, where $a_1 * x$ denotes the one-dimensional convolution of a_1 and x.

Detection of the three corners is achieved using the method proposed in (*13*), a method that approximates plane curves using B-splines and detects corners by locating local curvature maxima. Since the corner detection method is discussed in detail in (*13*) we present only the basic idea in a somewhat simplified form. Given four adjacent pixels P_{i-1}, P_i, P_{i+1}, P_{i+2} on the boundary curve b_s, we approximate this curve segment using cubic B-spline interpolation, resulting in the interpolated curve segment shown in Fig. 4. For curve segments with low curvature the distance δ_i between point P_i and the interpolated point P_i' is small and the estimated curvature c_i at P_i is also small. Conversely, a point P_i can be classified as a corner-point if the following criteria are met:

1. the distance δ_i exceeds a threshold value T_δ;
2. the estimated curvature c_i exceeds a threshold value T_c;
3. the estimated curvature c_i is a local maximum.

In addition, since we are looking for three control-points only, we select the three corners with maximum curvature c_i as control-points for alignment.

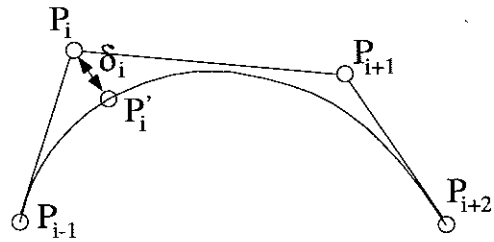

FIG. 4. Illustration of the breast boundary interpolation method. Four points $P_{i-1}, \ldots, P_{i+2}$ on the boundary are interpolated using cubic B-spline interpolation, resulting in a smooth interpolation curve. The distance δ_i between point P_i and the interpolated point P'_i is used to determine corner-points.

Inspection of the breast boundary in Fig. 2 shows that multiple corner-points could be used to locate the nipple-point. Protrusion of the nipple, however, is found only in a small fraction of all mammograms. On the other hand, it must also be ensured that only a single corner-point is found at the nipple. This is achieved by making the averaging kernel [4] large enough, so that the local structure of the boundary at the nipple-point is smoothed out.

Experimental results with a large set of mammograms showed that, for a majority of mammograms, the three extracted control-points indeed correspond to the nipple-point and the two corner-points between breast boundary and chest wall. In mammograms where this was not the case, one or more control-points were entered manually.

D. Alignment

The mammogram alignment method is best explained using the illustration in Fig. 3. Given the three control-points C_1–C_3, alignment of the left and right breast areas is achieved in four steps. First, one mammogram is rotated so that the orientations of the baselines $\overline{C_1C_3}$ match. Second, both mammograms are aligned on the point C_m, midway between C_1 and C_3. Now let the angle between the baselines $\overline{C_1C_3}$ and the centerlines $\overline{C_mC_2}$ be denoted by θ_L and θ_R, for the left and right breast, respectively. In the third step, one mammogram is transformed to obtain $\theta_L = \theta_R$. This is achieved by shifting the pixels in subregions A and B of one mammogram by an appropriate amount in the direction of the baseline $\overline{C_1C_3}$. For a row of pixels at a distance d from the baseline $\overline{C_1C_3}$ the amount of shift is given by $d(\cot \theta_L - \cot \theta_R)$.

The final step of the alignment process is designed to compensate for possible differences in size and shape. Up to this point one mammogram has been translated (the baseline centers C_m are aligned), rotated (the orientations of the baselines $\overline{C_1C_3}$ match), and skew differences have been eliminated (the orientations θ_L and θ_R of the centerlines $\overline{C_mC_2}$ match). In the following description we assume, without loss of generality, that the baselines $\overline{C_1C_3}$ are horizontal. The

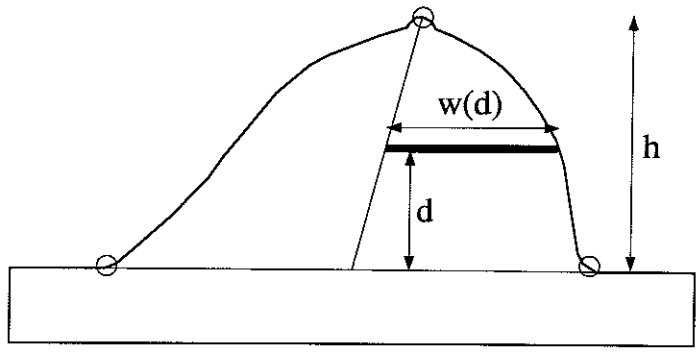

FIG. 5. Schematic outline of a breast area showing a (black) row of pixels at a distance d from the baseline and a width $w(d)$ between center line and breast boundary. Also indicated is h, the distance between the baseline and the nipple-point.

subregions A_L and A_R (as well as B_L and B_R) still can differ both in height h and width $w(d)$, the distance between centerline and the breast boundary, at a distance d from the baseline (see Fig. 5). Using the ratios h_R/h_L and $w_R(d)/w_L(d)$ all pixels of the left breast area can be mapped into the right breast. The row of pixels indicated in black in Fig. 5 is mapped into the right breast by translating it vertically to a position $d \cdot h_R/h_L$ away from the baseline and by scaling it horizontally by a factor $w_R(d)/w_L(d)$. The transformed coordinates may not be integers, so a pixel-by-pixel correspondence is obtained through bilinear interpolation (*14*).

This completes the process of mammogram alignment. The result of the alignment process for the mammograms in Plate 1 are shown in Plate 2. Points with the same coordinates in the left and right mammogram are now considered to correspond to each other. We can now test corresponding regions in the left and right breasts for the presence of structural asymmetries.

III. ASYMMETRY DETECTION

Tumor detection using the asymmetry method involves the detection of "structural asymmetries" between corresponding regions in the left and right breasts. Unfortunately, the term "structural asymmetry" is not defined precisely. In fact, it could be defined along a whole range of abstractions. At one extreme of this range, one could define any grey-level difference between pixels of corresponding regions as constituting an asymmetry. Such definition would clearly stand at odds with the observations that corresponding regions are hardly ever identical, either due to natural asymmetries between the two breasts or due to variations in the mammographic recording procedure. At the other extreme, one could attempt to identify and characterize all anatomical structures within the breast area and then detect asymmetries based on these descriptions. The drawback of this approach, apart from its complexity, is that a full descrip-

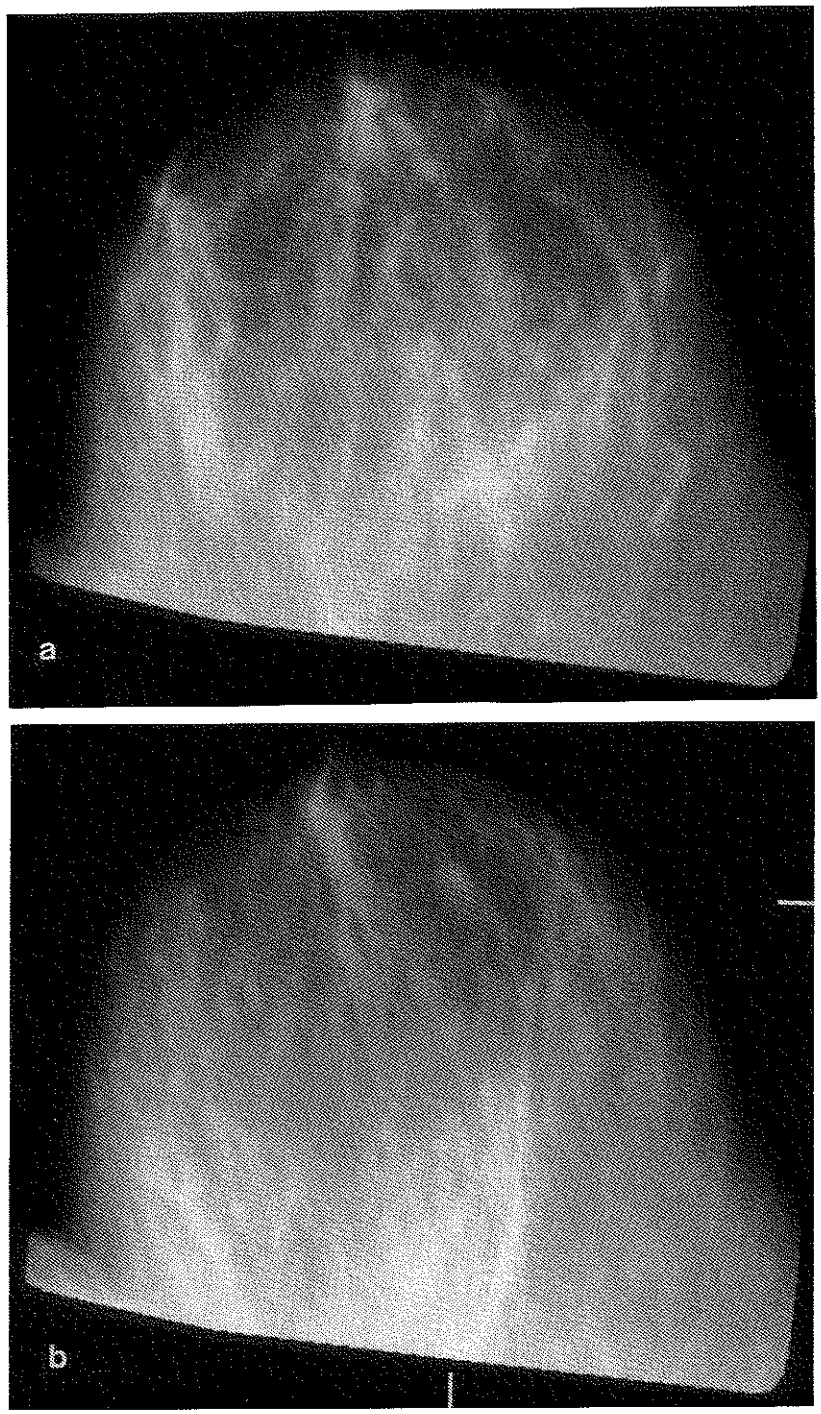

PLATE 2. Mammograms of the left and right breast after mammogram alignment. The tumor position is indicated by the two white lines.

tion of anatomical structures would include a description of tumor-related structures. But it is exactly these structures we wish to detect using the asymmetry approach.

For these reasons, we use a set of measures that are somewhere between the two extremes just discussed. On the one hand, they have to be related to the mammographic appearance of tumors; on the other hand, no characteristics of specific tumors are used for asymmetry detection. Finally, it is the combination of these measures that defines what we mean by "structural asymmetry."

In the following, we develop a set of increasingly complex structural measures for describing image regions and for detecting asymmetries between corresponding regions in the left and right breasts. Each measure is briefly motivated; its implementation is described and its performance for the mammogram in Plate 1 is shown. A full evaluation of their performances is, however, given only in the last section.

A. Brightness

Cancer cells have a higher density than healthy breast tissue and thus appear brighter in mammograms. Consequently, large grey-level differences between corresponding regions can indicate the presence of a tumor. The simplest way to detect grey-level differences is to subtract digitally the aligned mammograms (*10, 12*). However, there are several arguments that speak against simple subtraction. First, there are usually global differences in brightness and contrast between the left and right mammogram, due to variations in the mammographic recording procedure and in mammogram digitization. These differences, in turn, would be interpreted as asymmetries by the simple subtraction method. To avoid this problem, mammograms are first normalized. Given a digitized mammogram $M(x,y)$, the normalized mammogram $N(x,y)$ is defined as $N(x,y) = (M(x,y) - \mu_M)/\sigma_M$, where μ_M is the mean grey-level and σ_M is the standard deviation of grey-levels of M.

Second, even if there were identical anatomic structures in corresponding regions, inaccuracies in mammographic alignment would lead to a response in the pixel-by-pixel digital subtraction. Furthermore, differences in brightness are assumed to occur on a larger scale than the resolution of a single pixel. Therefore, brightness differences are measured for local grey-level averages. More precisely, given an averaging filter $a_2(x,y)$ as defined in Eq. [2], the brightness difference measure $B(x,y)$ is defined as

$$\begin{aligned} B(x,y) &= |N_L(x,y) * a_2(x,y) - N_R(x,y) * a_2(x,y)| \\ &= |(N_L(x,y) - N_R(x,y)) * a_2(x,y)|, \end{aligned} \qquad [5]$$

where N_L and N_R denote the left and right normalized mammogram, and $*$ denotes convolution.

The brightness difference for the mammogram in Plate 1, using an averaging filter with $n = 5$, is shown in Plate 3a. It is clear from the result that the brightness-difference measure responds to a variety of image phenomena and

that the response to the tumor present in the mammograms is in fact very small. However, the difference measure proved useful in many other cases, as is reported in Section IV.

B. Roughness

Tumors appear mammographically as brightness patterns different from healthy tissue. That is, within local regions, brightness variations follow different patterns for tumors and for healthy tissue. It should therefore be possible to discriminate tumors from non-tumors using texture measures. In the past, several groups have shown that such measures can successfully be used for mammographic diagnosis (*4, 6, 10*). One problem with the use of texture measures is the difficulty in determining what specific measures are likely to be good discriminators between tumors and non-tumors. If only certain tumors have to be detected, one can use measures designed to respond to the specific characteristics of that tumor, such as, for example, the "star-likeness" measure used by (*4*). However, as the number of texture measures is increased to cover different types of tumors, so does the probability that one or more of these measures respond in regions of healthy tissue. Therefore we can expect an increasing rate of false positives.

For these reasons, we have restricted the use of texture measures to a few whose usefulness for tumor detection can be justified easily. The first one, presented in this section, is a local variance measure to characterize roughness of local brightness patterns. A majority of tumors can be expected to produce a local increase in brightness variance: Microcalcifications, for example, appear as clusters of tiny, bright and sharp spots on a darker background. Similarly, the structure of stellate lesions leads to a higher local variance in brightness. Finally, the variance measure also responds to well-defined edges thus yielding a strong response at edges of circumscribed masses.

Local variance measures are dominated by areas with large variations in brightness. Their response is weak for a region with little grey-level variation, even if its surround is homogeneous. But this is precisely a situation found with tumors embedded, for example, in fatty tissue which has very little grey-level variation. If the breast area also contains, for example, glandular tissue with high grey-level variation, these tumors remain undetected. To overcome this problem, we use a variance measure that is locally normalized within a normalization window W. Given a variance window V and a (larger) normalization window W, with variances σ_V^2 and σ_W^2, respectively, the normalized local variance at (x,y) is defined as

$$v(x,y) = \sigma_V^2/\sigma_W^2. \qquad [6]$$

Finally, the roughness difference $R(x,y)$ between two corresponding regions in the left and right breasts are defined as

$$R(x,y) = |v_L(x,y) - v_R(x,y)|, \qquad [7]$$

where v_L and v_R are the normalized local variances of N_L and N_R, respectively.

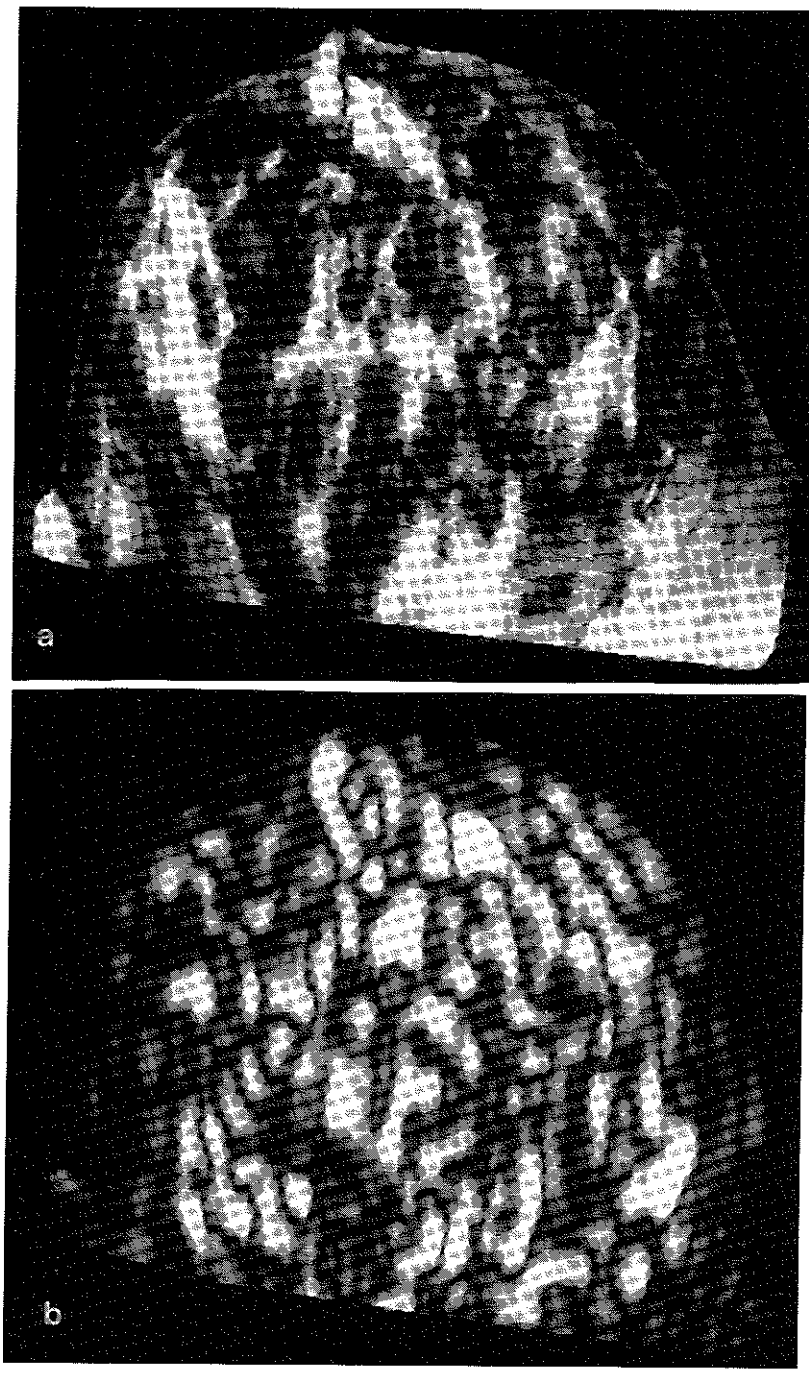

PLATE 3. Response of the asymmetry measures to the mammograms of Plate 2: (a) Response of the brightness difference measure B. (b) Response of the roughness difference measure R. (c) Response of the brightness-to-roughness difference measure Q. (d) Response of the combined asymmetry measure A.

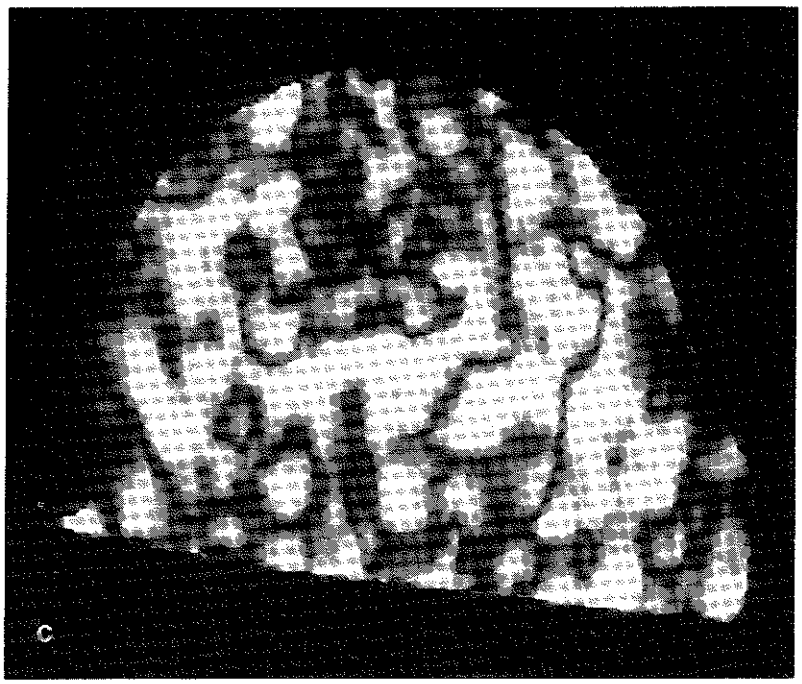
c

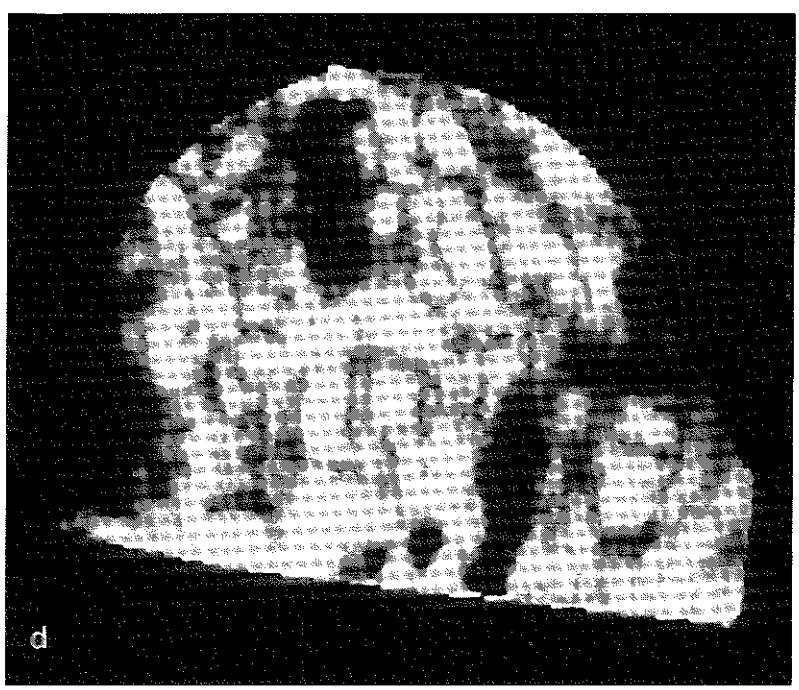
d

TABLE 1

COMPARISON OF BRIGHTNESS AND ROUGHNESS FOR DIFFERENT TYPES OF TISSUE

	Tumor	Glandular tissue	Fatty tissue
Brightness	High	Medium-high	Low
Roughness	Low	High	Low
Brightness/roughness	High	Low	Low

The response of the roughness difference measure $R(x,y)$ for the mammogram in Plate 1 is shown in Plate 3b, using a variance window of size 25 × 25 pixels, and a normalization window of size 51 × 51 pixels. Detection performance of the roughness measure is best for relatively small tumors embedded in a homogeneous background. It is poor for very large tumors, if the corresponding region in the other breast is homogeneous.

C. Brightness-to-roughness

Large tumors cannot be detected by either the brightness or the roughness measure alone if the corresponding region in the other breast is homogeneous. This occurs, for example, if the corresponding region contains fatty tissue or glandular tissue. A comparison of the three types of tissue is given in Table 1. From that description, it can be seen that the brightness-to-roughness ratio can be a good discriminator between tumors and other tissues.

The brightness-to-roughness ratio could be implemented using the brightness and variance measures presented in the previous sections. The variance measure is, however, too general since it responds both to rough textures and to edges. This suited our purpose for the situations described in the last section, but here we need a measure that responds more specifically to roughness. This is achieved by defining roughness within a $n \times n$ window W using the running sum of absolute grey-level differences in both the vertical and horizontal directions. Let

$$p_j = \frac{1}{n^2} \sum_{(x,y)\in W} (h_j(x,y) + v_j(x,y)), \qquad [8]$$

where

$$h_j = \begin{cases} 1, & |M(x+1,y) - M(x,y)| = j \\ 0, & \text{otherwise} \end{cases} \qquad [9]$$

$$v_j = \begin{cases} 1, & |M(x,y+1) - M(x,y)| = j \\ 0, & \text{otherwise.} \end{cases}$$

Then roughness can be defined as

$$\sigma_W = \sum_{j=0}^{255} j^2 p_j, \qquad [10]$$

and the brightness-to-roughness ratio for a window W centered at (x,y) is defined as

$$q(x,y) = \mu_W^2/(1 + \sigma_W), \quad [11]$$

where μ_W is the average grey-level within the window W. Finally, the brightness-to-roughness difference is defined as

$$Q(x,y) = |q_L(x,y) - q_R(x,y)|, \quad [12]$$

where q_L and q_R are the brightness-to-roughness ratios for the left and right breasts, respectively.

The response of this measure for the mammogram in Plate 1 is shown in Plate 3c, and for a large tumor in Plate 4. Experiments with a large set of mammograms showed that the brightness-to-roughness difference Q responded strongly to a majority of large tumors.

D. Directionality

An analysis of the response patterns generated by the asymmetry measures presented in the previous sections reveals that they respond to structures other than tumors. Strong responses are also generated in regions with blood vessels or with glandular tissue. These regions typically appear as highly oriented patterns that are predominantly oriented in a direction orthogonal to the baseline (see Fig. 3). Tumors, on the other hand, rarely appear as highly oriented patterns, at least not at the level of resolution at which we are analyzing mammograms. This permits the formulation of the following rule: If a region contains a highly oriented pattern, oriented orthogonally to the base line, then it is unlikely that a response of the asymmetry measures is due to the presence of a tumor. Therefore, the response of these measures should be suppressed in regions with highly oriented patterns.

In the following description we assume that the baseline $\overline{C_1C_3}$ is horizontal (see Fig. 3). Let $F(u,v)$ denote the discrete Fourier transform of the brightness profile within a window W and let $P(u,v)$ denote the power spectrum, i.e., $P(u,v) = F(u,v)F^*(u,v)$, where $F^*(u,v)$ denotes the complex conjugate of $F(u,v)$. The support of the power spectrum is shown in Fig. 6. All frequency components in the shaded area have a predominantly vertical orientation. Let P_V denote the total power in the shaded area and P_W denote the total power in the window W. Then vertical directionality can be defined as $D = P_V/P_W$. For non-oriented patterns D is approximately $\frac{1}{2}$; for highly oriented, vertical patterns D is close to 1, and for highly oriented, horizontal patterns D is close to 0.

Now we can reformulate the rule given before: If in a window W, D is close to 1, then it is unlikely that a strong response of the asymmetry measures is due to the presence of a tumor. Therefore, the directionality measure can be used as a weighting factor for the asymmetry measures. This is described in the next section.


a

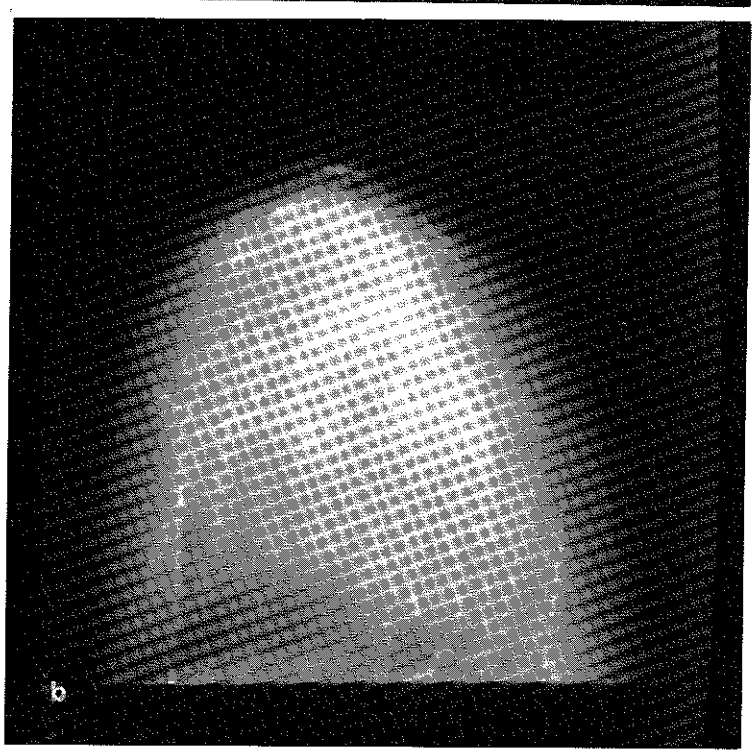
b

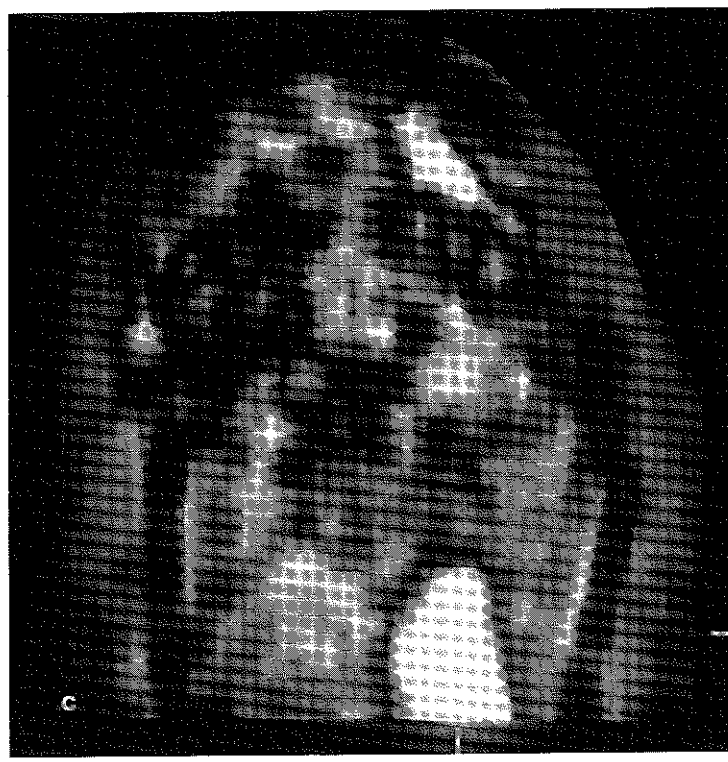

PLATE 4. Mammograms of left (a) and right (b) breast containing a very large tumor, and response (c) of brightness-to-roughness difference measure Q. The tumor position is indicated by the two white lines.

The main advantage of the power spectral method lies in the fact that it can, to a certain extent, measure local directionality in a resolution-independent way. Its major disadvantage is the large computational cost. (The asymmetry measures introduced above can be computed very efficiently using sliding summation methods (*15*).) For this reason, the directionality measure was computed on a reduced-resolution version of the digitized mammograms $M(x,y)$, and the power spectra were computed for a relatively small window size of 16 × 16 pixels.

E. Asymmetry Measurement

In the previous sections we introduced three measures that capture different types of asymmetries, namely brightness (B), roughness (R), and brightness-to-roughness (Q). A fourth measure, directionality (D), was introduced to suppress the response of the other measures in regions containing highly oriented structures, such as blood vessels or glandular tissue. We now discuss how these measures are combined into a single asymmetry measure.

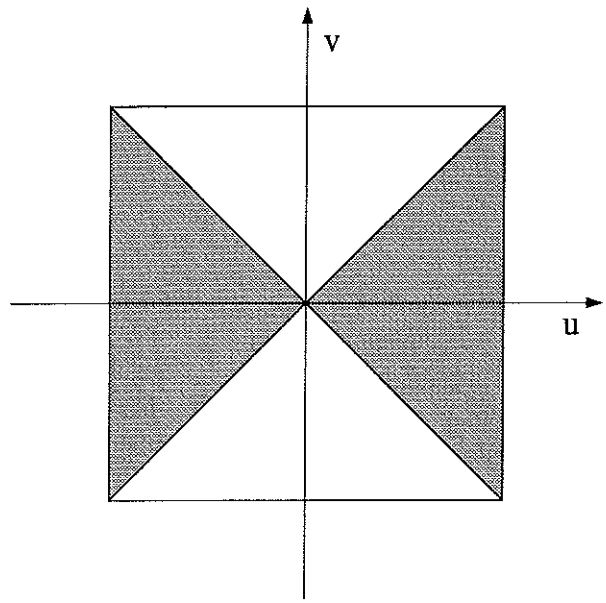

FIG. 6. Support of the power spectrum used in computing the directionality measure D. The frequency components in the shaded area have a predominantly vertical orientation.

The directionality measure D should be used very conservatively in suppressing responses of other measures: only where the values of D are extreme, should suppression be noticeable. This is achieved through a non-linear transformation in the following way. A weighting factor $W(x,y)$ is defined as

$$W(x,y) = \max [0,1 - D_p(x,y)], \quad [13]$$

with

$$D_p(x,y) = D_L^p(x,y) + D_R^p(x,y), \quad [14]$$

where D_L and D_R are the directionality measures for the left and right breasts, both raised to the pth power. Experimental results showed that a value of $p = 5$ produced good results. The asymmetry measure $A(x,y)$ is then defined as

$$A(x,y) = [B(x,y) + R(x,y) + Q(x,y)] * W(x,y). \quad [15]$$

The asymmetry measure $A(x,y)$ combines all asymmetry measures in a simple, unweighted manner. It defines what is considered as a "structural asymmetry" in our system. This concludes the definition of our asymmetry measurement. The response of the asymmetry measure A for the mammogram in Plate 1 is shown in Plate 3d. In the next section we present experimental results obtained with this measure for a set of mammograms.

IV. Experimental Results and Discussion

The methods presented here were tested with a set of 10 mammogram pairs that had not been used in the training phase. These mammograms contained a total of 13 areas with either a tumor or with strong signs for the possible presence of a tumor (suspicious areas). The set of test cases is quite small because we used only cases where "structural asymmetry" played a major role in the radiologist's diagnosis. The tests reported in this section should therefore not be compared to a clinical evaluation. On the other hand, the method presented here is not intended to be used alone for cancer diagnosis, but rather as one in a set of methods for locating suspicious areas, as was discussed in the Introduction.

Given a response pattern of the asymmetry measure, such as shown in Plate 3d, we must first devise a method for selecting suspicious areas. Since all regions having a strong left–right asymmetry are considered suspicious, we could simply diagnose all positions as suspicious where A exceeds a certain threshold. This simple thresholding suffers from the problem that there is no prior knowledge for selecting a reasonable threshold value.

For this reason, we use a two-stage thresholding method for selecting suspicious areas from A. First, a percentile method is used to select potential tumor sites, i.e., a fixed percentage of locations is classified as potentially suspicious. A threshold T_1 is chosen such that q_1 percent of all positions in A exceed T_1. This is based on the assumption that tumors occupy an area at most q_1 percent of the total breast area. The potentially suspicious positions are then further analyzed to reduce the number of false positives.

We assume that the asymmetry measure responds not only at the center of a tumor but also in the immediate neighborhood of the center. Using blob coloring (*16*), we identify clusters of asymmetry responses. If the area of a cluster is too small, the cluster is eliminated. Otherwise, a circle is fitted around the cluster and the mean response within the circle is computed. Let A_{max} be the maximum mean response of all potentially suspicious areas. A second threshold T_2 is chosen such that $T_2/A_{max} = q_2$. All potentially suspicious areas whose mean response does not exceed T_2 are eliminated from the list of suspicious areas. All other areas are considered suspicious and are reported by the program.

In comparing the results produced by the computer and the diagnoses given by the radiologist, we cannot expect that the suspicious areas found are exactly the same. Therefore, the following criterion was adopted. The radiologist drew a circle around each suspicious area. If the intersection of this circle with the nearest area indicated by the computer overlapped more than 50%, the suspicious area was considered detected, otherwise is was considered missed.

The two parameters q_1 and q_2 were determined as follows. Parameter q_1 was varied over a large range and a value of $q_1 = 5\%$ was found to produce the best result. Similarly, parameter q_2 was varied, and these results are shown in Table 2. It is clear that in selecting a value for q_2 there is a trade-off between the numbers of false positives and misses. A low value of q_2 produces many false

TABLE 2

HIT RATE AND FALSE POSITIVES FOR DIFFERENT VALUES OF THRESHOLD q_2

Threshold (%)	Hit rate (%)	Average number of false positives per mammogram
70	92	9.9
80	92	4.9
90	69	1.6

positives, and a high value produces many misses. A good compromise was found for $q_2 = 80\%$.

The final results show that, for the set of mammograms analyzed, 12 out of 13 suspicious areas were detected, and that, on the average, 4.9 false positives were generated per mammogram pair. This indicates that the asymmetry method is indeed sensitive enough to be used in an automated tumor-detection system. The results also show that the asymmetry method *alone* is not reliable enough for clinical application. First, although the false positive rate of 4.9 compares favorably with other methods reported in the literature (e.g., (*4*)), it still means that several asymmetry positions are signaled in every mammogram. Second, the asymmetry method cannot provide any tumor classification. These results are in line with the expectations formulated in the Introduction. A system for mammographic diagnosis must rely on multiple cues for achieving reliable detection performance. The asymmetry method can provide cues not available to other methods and thus can improve the performance of such systems.

ACKNOWLEDGMENTS

This work was supported by the Canadian Natural Sciences and Engineering Research Council under Grants OGP38521 and EQP42012. We thank V. Di Lollo for helpful comments.

REFERENCES

1. SADOWSKY, N., AND KOPANS, D. B. Breast cancer. *Radiol. Clin. N. Am.* **21,** 51 (1983).
2. TABÁR, L., AND DEAN, P. B. The control of breast cancer through mammography screening. *Radiol. Clin. N. Am.* **25,** 961 (1987).
3. LAI, S. M., LI, X., AND BISCHOF, W. F. On techniques for detecting circumscribed masses in mammograms. *IEEE Trans. Med. Imag.* **8,** 377 (1989).
4. HAND, W., SEMMLOW, J. L., ACKERMAN, L. V., AND ALCORN, F. S. Computer screening of xeromammograms: A technique for defining suspicious areas of the breast. *Comput. Biomed. Res.* **12,** 445 (1979).
5. KIMME, B., O'LOUGHLIN, B. J., AND SKLANSKY, J. Automatic detection of suspicious abnormalities in breast radiographs. *In* "Data Structure, Computer Graphics and Pattern Recognition" (A. Klinger, K. Fu, and T. Kunii, Eds.), pp. 427–447. Academic Press, New York, 1975.
6. SEMMLOW, J. L., SHAAGOPAPPAN, A., ACKERMAN, L. V., HAND, W., AND ALCORN, F. S. A fully automated system for screening xeromammograms. *Comput. Biomed. Res.* **13,** 350 (1980).
7. MAGNIN, I. E., CLUZEAU, F., AND ODET, C. L. Mammographic texture analysis: An evaluation of risk for developing breast cancer. *Opt. Eng.* **25,** 780 (1986).

8. NG, S. L. "Breast Cancer Diagnosis by Computer." Master's thesis, The University of Alberta, 1990.
9. CHAN, H.-P., DOI, K., GALHOTRA, S., VYVORNY, C. J., MACMAHON, H., AND JOKICH, P. M. Image feature analysis and computer-aided diagnosis in digital radiography. I. Automated detection of microcalcifications in mammography. *Med. Phys.* **14,** 538 (1987).
10. ACKERMAN, L. V., AND GOSE, E. E. Breast lesion classification by computer and xeroradiograph. *Cancer* **30,** 1025 (1972).
11. SMITH, K. T., WAGNER, S. L., GUENTHER, R. B., AND SOLMON, D. C. The diagnosis of breast cancer in mammograms by the evaluation of density patterns. *Radiology* **125,** 383 (1977).
12. ZHOU, X., AND GORDAN, R. Geometric unwarping for digital subtraction mammography. In "Proceedings of Vision Interface '88," pp. 25–30. Canadian Image Processing and Pattern Recognition Society, Edmonton, Alberta, Canada, 1988.
13. MEDIONI, G., AND YASUMOTO, Y. Corner detection and curve representation using cubic *B*-splines. *Comput. Vision Graphics Image Process.* **39,** 267 (1987).
14. ROSENFELD, A., AND KAK, A. C. "Digital Picture Processing," Vol. 2. Academic Press, New York, 1982.
15. YAROSLAVSKY, L. P. "Digital Picture Processing." Springer-Verlag, Berlin, 1985.
16. BALLARD, D. H., AND BROWN, C. M. "Computer Vision." Prentice Hall, Englewood Cliffs, NJ, 1982.